MATERIALS CHEMISTRY FRONTIERS

Hydrogen Bonding Directed Co-Assembly of Polyoxometalates and Polymer to Core-Shell Nanoparticles

Journal:	*Materials Chemistry Frontiers*
Manuscript ID	QM-RES-06-2018-000291.R1
Article Type:	Research Article
Date Submitted by the Author:	09-Aug-2018

Complete List of Authors:	Zhou, Jing; University of Akron, Hu, Jie; Nanchang University, Chemistry Li, Mu; South China University of Technology Li, Hui; the University of Akron Wang, Weiyu; South China University of Technology Liu, Yuzi; Argonne national Laboratory, Center for Nanoscale Materials Winans, Randall; Argonne National Laboratory, Li, Tao; Argonne National Lab, Liu, Tianbo; University of Akron, Department of Polymer Science Yin, Panchao; South China University of Technology, South China Advanced Institute for Soft Matter Science and Technology; Oak Ridge National Laboratory,

Journal Name

ARTICLE

Hydrogen Bonding Directed Co-Assembly of Polyoxometalates and Polymer to Core-Shell Nanoparticles†

Received 00th January 20xx,
Accepted 00th January 20xx

DOI: 10.1039/x0xx00000x

www.rsc.org/

Jing Zhou,[ab] Jie Hu,[a] Mu Li,[a] Hui Li,[b] Weiyu Wang,[a] Yuzi Liu,[c] Randall E. Winans,[d] Tao Li,*[de] Tianbo Liu,*[b] and Panchao Yin*[a]

A general strategy has been developed here to co-assemble polyoxometalates (POMs) and polymers into core-shell hybrid nanoparticles *via* hydrogen bonding interaction. Due to the hydrogen bonds between the pyridine groups of poly(4-vinyl pyridine) (P4VP) and the hydrogen bonding donor groups on the POM surface, P4VP is stabilized by the POMs and dispersed as discrete hybrid core-shell nanoparticles in aqueous solution. For these thermodynamically stable nanoparticles, the P4VP cores are covered with hexagonally closed packed POMs. The size of core-shell particle is controlled by the electrostatic repulsive interaction among the POMs. The introduction of extra salts screens the repulsive force among the POMs, thus increasing the size of the core-shell structures.

Introduction

Due to their rich phase behaviours in both bulk state and solution, polymers have been widely applied in templating the synthesis of nanoparticles (NPs) with various morphologies and directing the assembling of NPs into hierarchically ordered structures.[1-9] Polymers can covalently graft on the surface of NPs with high stability. The obtained hairy NPs show tuneable mechanic properties, better processability, and enhanced compatibility with organic media.[10-14] However, the complex synthesis and high cost of purification limit their applications. Non-covalent interactions, including van der Waals forces, hydrophobic interaction, hydrogen bonding, aromatic stacking and electrostatic interaction, have been employed as driving forces to assemble the polymer-NP complex structures.[3, 16-23] This protocol is feasible from the aspect of synthesis and can build self-healing materials and smart materials that are responsive to external stimulus due to the dynamic nature of the non-covalent bonding.[9, 20] The search of appropriate polymers and NPs with required surface ligands is the key to this protocol. However, the rational design of non-covalently interacted NP/polymer systems is currently beyond our knowledge. A thorough understanding of the non-covalent interactions is critical to design the building blocks and tune the strength of the polymer template/NP interactions.

Polyoxometalates (POMs) are a group of well-defined, nano-scaled molecular clusters composed of early transition metal centers and oxo ligands with tuneable morphologies and surface charge density.[24-26] Different from regular NPs, POMs are monodispersed in both solid state and solutions.[24-26] Their structures, including surface structures, are well defined and characterized at atomic level, providing model systems for the study of supramolecular assemblies of nano-scaled objects.[26-28] The surface of POMs is mainly composed of oxo, hydroxyl, and/or water ligands, providing access to the formation of hydrogen bonding.[27] The anionic feature of POMs facilitates the study of their electrostatic interaction with cationic molecules.[28] As specific examples, POM-organic hybrid materials have been designed to self-assemble into 1D structure *via* the formation of hydrogen bonding network.[27] Meanwhile, the interaction between anionic POMs and cationic surfactants or polymers leads to the formation of nanostructures with various morphologies.[28] Based on the charge interaction between poly(4-vinyl-*N*-methylpyridinium iodide), micelles and vesicles with tuneable sizes can be conveniently prepared.[29, 30] Therefore, using POMs as models to explore the effect of non-covalent interactions in polymer/NP co-assembly system is advantageous. Meanwhile, the applications of POMs have been significantly developed and broadened these years in the fields of catalysis, medicine, electronic memory devices and single molecular magnets.[31-35] The polymer-templated assembly of POMs protocol provides a rational way to extend their practical applications, e.g. high efficient heterogeneous catalysis and functional devices.

[a] South China Advanced Institute for Soft Matter Science and Technology & State Key Laboratory of Luminescent Materials and Devices, South China University of Technology, Guangzhou 510640, China
[b] Department of Polymer Science, The University of Akron, Akron, Ohio 44325-3909, USA
[c] Center for Nanoscale Materials, Advanced Photon Source, Argonne National Laboratory, Argonne, Illinois 60439, USA
[d] X-ray Science Division, Advanced Photon Source, Argonne National Laboratory, Argonne, Illinois 60439, USA
[e] Department of Chemistry and Biochemistry, Northern Illinois University, DeKalb, Illinois 60115, USA
† E-mail: taoli@aps.anl.gov; tliu@uakron.edu; yinpc@scut.edu.cn
‡ Electronic Supplementary Information (ESI) available. See DOI: 10.1039/x0xx00000x

Herein, we reported the synthesis, structural characterization, and the formation mechanism of the core-shell NPs with polymer cores and close-packed POM shells. Poly(4-vinylpyridine) (P4VP) was used as the template materials to form complex with 5 POM clusters with different topologies and charge densities, respectively. The morphologies of obtained NPs complexes were studied by electron microscopy and scattering techniques while the non-covalent interaction between POMs and polymer were probed by vibration spectroscopy and scattering techniques.

Results and Discussion

Synthesis of POM-P4VP complex

The synthesis of POM-P4VP complex was convenient and straightforward by mixing the ethanol solutions of P4VP with the aqueous solutions of POMs (Figure 1a). In a typical synthetic experiment, 0.5 mL solution of P4VP (M_w = 60 KDa) in ethanol (2 mg/mL) was added drop-wisely to 10 mL aqueous solutions of POMs at different concentrations (Figure 1). The resulted solutions were kept to open air and stirred for 1 day until ethanol evaporated. The solution turned to cloudy and formed precipitation when the molar ratio of POM/P4VP was below 5. Scanning electron microscopy (SEM) analysis of the precipitates showed they formed irregular aggregates in the mixture process (Figure 2a). When larger amount of POMs was introduced in the reaction, clear and stable solutions were obtained (molar ratio of POM/P4VP ≥ 5). P4VP, soluble in polar organic solvents, shows poor solubility in water and is considered as a hydrophobic polymer. Being similar to the formation of Pickering emulsion, water-soluble POMs can be used to stabilize P4VP in aqueous solutions to reduce the surface energy of P4VP in water, which eventually lead to the formation of thermodynamically stable solutions. A certain amount of POMs was required to fully protect the P4VP surface for high solubility and stability. The clear solution obtained after POM/P4VP complexation were investigated by dynamic light scattering (DLS) technique. The results showed the formation of large nanoparticles with narrow size distribution (see Figures S1 to S3 in ESI‡). More importantly, as a general synthetic protocol, it was successfully applied to prepare stable POM/P4VP complex with 5 POM clusters with various sizes, including {SW}[36](formula: $H_{50}Na_{10}O_{135}S_5W_{30}$; size: 1.5 nm X 1 nm); {PW}[37] (formula: $K_{14}NaP_5W_{30}O_{110}\bullet 31H_2O$; size: 1.5 nm X 1 nm, plate-shape), {$Mo_{72}V_{30}$}[38] (formula: $Na_8K_{14}(VO)_2[\{Mo_6O_{21}(H_2O)_3\}_{10}\{Mo_6O_{21}(H_2O)_3(SO_4)\}_2\{VO(H_2O)\}_{20}(VO)_{10}(\{KSO_4\}_5)_2]\bullet$ca. $150H_2O$; size: 2.5 nm, hollow sphere), {$Mo_{72}Fe_{30}$}[39] (formula: $[Mo_{72}Fe_{30}O_{252}(CH_3COO)_{12}\{Mo_2O_7(H_2O)\}_2\{H_2Mo_2O_8(H_2O)\}(H_2O)_{91}]\bullet$*ca.*$150H_2O$; size: 2.5 nm, hollow sphere), and {Keg}[40] (formula: $H_3PW_{12}O_{40}$; size: 1 nm, solid sphere) (Figures 1, 2, and Figures S2 to S8 in ESI‡).

The structure of POM-P4VP complex

The clear solutions of POM/P4VP were further studied by transmission electron microscopy (TEM) to probe the structural details of the formed complex NPs. In a typical TEM study, spherical nanoparticles were observed in the samples prepared from the clear solutions of POM/P4VP mixtures. The average sizes of the nanoparticles measured from the TEM images were consistent with the corresponding the size information obtained from DLS studies (Figure 2, and Figures S2 to S8 in in ESI‡). In a magnified TEM images of a typical nanoparticle with a contrast close to the surface shown in Fig. 2c suggesting a core-shell model for the obtained nanoparticles. POM clusters, enriched with heavy metal ions, showed darker contrast than the domain of P4VP in TEM micrograph of Fig. 2c. Therefore, the inner core in the core-shell model was assigned to P4VP, which was crowded by layers of POMs. To further confirm the model, energy-filtered TEM (EFTEM) was applied to map the distribution of Fe and Mo in {$Mo_{72}Fe_{30}$}/P4VP complex shown in Fig. 2e and 2f, respectively, by three-window method. The complexation of {$Mo_{72}Fe_{30}$}/P4VP was used herein for EFTEM based on the follow consideration: there were two types of heavy metal ions in this POM, providing two different resources for tracking the distribution of POMs. These results not only assured the credibility of EFTEM results, but also affirmed the stability of POMs during the complexation process. The bright circle means there are a lot more Fe and Mo on the surface, which imply that POM is the major composition of shell structures. (Figures 2d, e, and f). Because of more Mo ions than Fe ions in each POM cluster (Mo/Fe = 72/30) and higher energy loss of Fe L edge, the Fe mapping signal is a lot lower than Mo's.

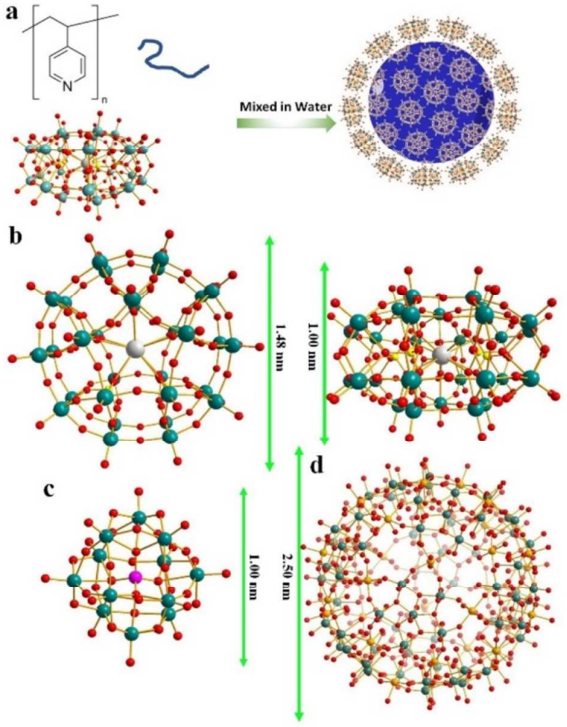

Figure 1. (a) Graphical representation of the polymer/POM complexation process; (b) top and side view of the molecular structures of {SW}/{PW}; (c) molecular structure of {Keg}; (d) molecular structure of {$Mo_{72}Fe_{30}$}/{$Mo_{72}V_{30}$}. Color codes for spheres: Teal, W; Red, O; Grey, K; Yellow, S for {SW} or P for {PW}; Orange, Fe for {$Mo_{72}Fe_{30}$} or V for {$Mo_{72}V_{30}$}.

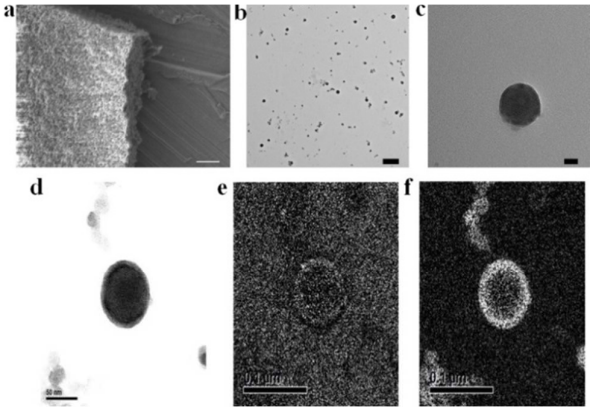

Figure 4. (a) SEM image of the precipitates formed in {SW}/P4VP complex solution (molar ratio of {SW}/P4VP = 1). Scale bar, 1 μm; b) TEM image of the NPs formed in {SW}/P4VP complex solution (molar ratio of {SW}/P4VP = 5). Scale bar, 200 nm; (c) Zoom in image of one NP in (b). Scale bar, 20 nm; (d) Bright field TEM image (scale bar, 50 nm), (e) Fe mapping (scale bar, 100 nm), and (f) Mo mapping (scale bar, 100 nm) of $\{Mo_{72}Fe_{30}\}$/P4VP complex NP.

Small angle X-ray scattering (SAXS) techniques, a powerful tool for characterization of nanostructure, were further utilized to explore the packing of POMs on the surface of P4VP cores.[41] The overall SAXS curve of the {SW}/P4VP complexation system showed the feature of poly-dispersed spheres with average sizes as *ca.* 60 nm (Figure 3a). Three interaction peaks at 0.40, 0.71 and 0.80 $Å^{-1}$ were observed at high Q range of the SAXS curve, indicating a hexagonal packing of {SW} on the surface of P4VP core with center to center inter-cluster distance as 1.80 nm (Figures 3a and b). Similar structures have been observed for the other polymer-virus systems.[42] The diameter of {SW} was 1.50 nm, suggesting the close contact of {SW} during their aggregation process on the surface of P4VP core. Such ordered packing on the polymer core surface was a general feature shared by the other POM/P4VP complexation system. The interaction peaks were also observed in the scattering curves of $\{PW_{12}\}$/P4VP and $\{Mo_{72}Fe_{30}\}$/P4VP complexes (Figure 3a). Due to their sizes differences among $\{PW_{12}\}$ (1.0 nm), {SW} (1.5 nm), and $\{Mo_{72}Fe_{30}\}$ (2.5 nm), the positions of their first interaction peaks shifted to low Q range, corresponding to the increasing of inter-POM distance ({Keg}/P4VP, 1.45 nm; {SW}/P4VP, 1.80 nm; $\{Mo_{72}Fe_{30}\}$/P4VP, 3.10 nm).

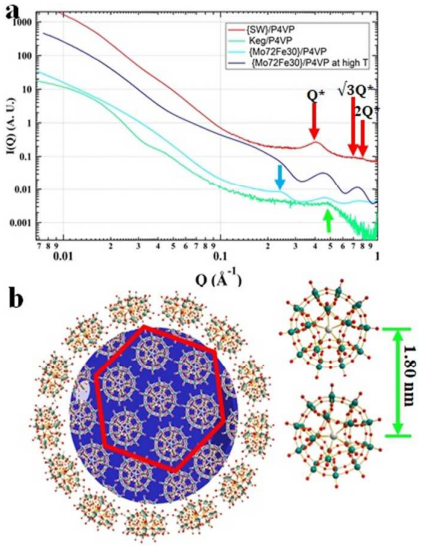

Figure 2. (a) SAXS data of concentrated solutions of {SW}/P4VP (red), $\{Mo_{72}Fe_{30}\}$/P4VP (blue), {Keg}/P4VP (green) at room temperature and $\{Mo_{72}Fe_{30}\}$/P4VP at 80 °C (light blue); (b) Graphical representation of the densely hexagonal packing of {SW} on the surface of P4VP core.

Driving force for POM/P4VP complexation

FT-IR techniques, as well as SAXS, were applied to probe the hydrogen bonding interactions between POMs and P4VP during their complexation process. Due to its well-defined hydrogen bond donor sites and corresponding well-studied vibration bands, the $\{Mo_{72}Fe_{30}\}$ system is selected for FT-IR studies.[43] In our previous study, we demonstrated that H-bonding and hydrophobic-hydrophobic interaction are the driving forces for the protein/polymer co-assembly.[18, 44] According to our previous studies, P4PV is mostly deprotonated at a pH>5. For most of POM solutions we prepared for complex nanoparticle preparation, their pH are above 5. Therefore, the contribution from the charge interaction between POMs with protonated P4VP is not the major drive force for the complexation process.[44] Because of the hydrophilic property of the POMs, we believe the hydrogen bonding is the main driving force for the assembly of P4VP and POMs.[45, 46] Hydrogen bonding interactions between the pyridine groups of P4VP and the hydroxyl/water groups on POMs surface were confirmed by FT-IR spectroscopy (Figure 4). The absorption peak at 3416 cm^{-1}, characteristic of hydroxyl groups in $\{Mo_{72}Fe_{30}\}$, shifted to 3427 cm^{-1} and became sharper and stronger because of the formation of hydrogen bonding (Figure 4a). The characteristic stretching vibration bands of C=N bond appeared at 1597 cm^{-1} and 1557 cm^{-1} for pure P4VP sample, respectively.[2] As evidence of the formation of hydrogen bonding, , the peak intensity at 1557 cm^{-1} decreased while the peak at 1597 cm^{-1} showed a clear shift to 1601 cm^{-1} for the corresponding spectrum of the complex sample (Figure 4c).[47-49] At the 950–1050 cm^{-1} region: the peak at 993 cm^{-1} of P4VP sample shifted to 1003 cm^{-1} in the complex samples with higher intensity (Figure 4b).[47-49] Meanwhile, SAXS was used to monitor the solution of $\{Mo_{72}Fe_{30}\}$/P4VP complex at high temperature. The sharp peak at 0.23 $Å^{-1}$ resulted from the interaction among

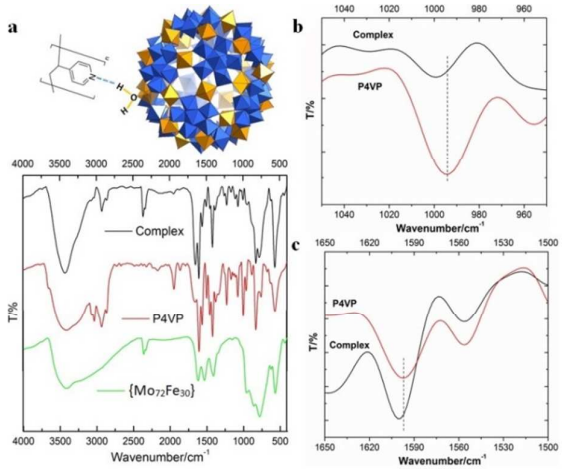

Figure 3. (a) the mode of hydrogen bonding formation between $\{Mo_{72}Fe_{30}\}$ and P4VP and the FT-IR spectra of $\{Mo_{72}Fe_{30}\}$, P4VP and their complex NPs; (b), (c) FT-IR spectra of P4VP and complex NP at selected region.

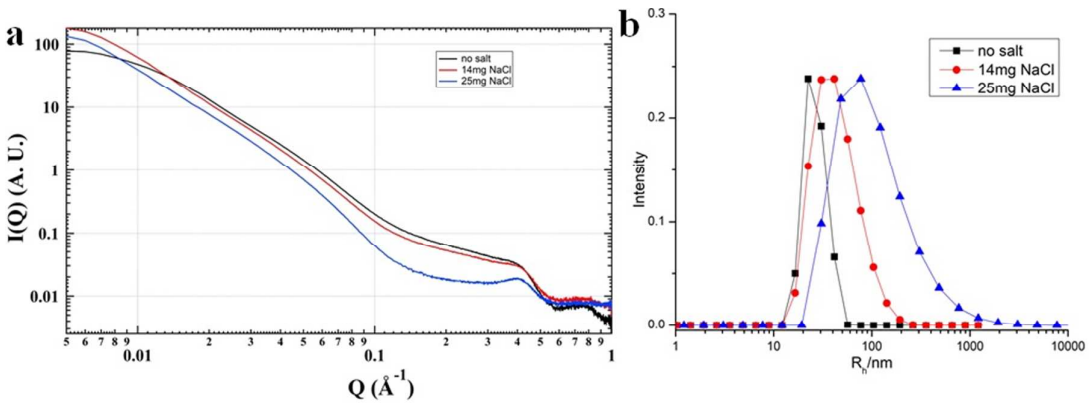

Figure 5. (a) SAXS and (b) light scattering studies of {PW}/P4VP system with the addition of different amounts of extra NaCl.

$\{Mo_{72}Fe_{30}\}$ on the surface of P4VP core disappeared when the solution temperature was elevated to 80 °C (Figure 3a). The overall particle size was observed to increase by analyzing the low Q range of the SAXS data, suggesting the disassembly of $\{Mo_{72}Fe_{30}\}$/P4VP complex (Figure 3a). At high temperature, the hydrogen bonds between $\{Mo_{72}Fe_{30}\}$ and P4VP were destroyed and the co-assemblies stabilized by these hydrogen bonding were disassembled, leading to the size increasing and finally precipitation of P4VP.[5, 50] This is different from previous studies on the charge interaction between positive charged poly(4-vinyl-*N*-methylpyridinium) Keggin type POMs. In this report, the hydrogen bonding interaction lead to the formation of core-shell nanoparticle while the charge interaction resulted in the formation of micelles and vesicles.[29, 30]

Further Justify the core-shell character of the POM/P4VP complex NPs

It is directly confirmed from the above structural analysis results that large NPs are formed in the complex aqueous solutions of POMs and P4VP with POMs close packed on the shells of NPs. The existence of P4VP in the final complex NPs is supported by the FT-IR results. The further justification that the cores of the complex NPs are made up of P4VP is mainly based on the hydrophobic nature of P4VP and the existence of hydrogen bonding between POMs and P4VP. In aqueous environment, the hydrophobicity of P4VP will drive the aggregation of P4VP to irregular precipitates. Therefore, to avoid contacting water, P4VP should be fully covered by hydrophilic POMs. Such process is energetically favored because of the multiple hydrogen bonding interaction between P4VP and POMs. It is, thus, natural to conject the core-shell picture of the P4VP-POM complex NPs.

Inter-POMs interactions on the surface polymer core

Most of POMs were highly negatively charged and repulsive with each other in solutions. In the aqueous solutions of POM/P4VP complex, POMs strongly interacted with each other with ordered packing on the surface of polymer core, which is similar to the packing of POMs on the surface of NPs.[51] The corresponding structure factors, sharp peaks, were observed in their SAXS data. With the addition of extra salt to the POM/P4VP complex solutions, the interaction peaks became sharper and shifted to high Q direction, suggesting the closer inter-POM distance in their ordered packing structures (Figure 5a). The introduction of additional salts resulted in the screening of repulsion among these negative charged POM clusters. Therefore, the inter-POM distance became shorter. Light scattering and TEM studies on these POM/P4VP core-shell structure indicated that the sizes of complex particle increase with the additional salt (Figure 5b and Figure S8 in ESI‡). The curvature of the POM/P4VP core-shell complex was defined by the repulsive interaction among POMs in the shell structures. The screening effect weakened the repulsion and decreased the curvature, leading to an increase in particle size.

Experimental Section

P4VP (Mw = 60 kDa), {Keg}, and ethanol were purchased from Sigma Aldrich and used without further purification. {SW}, {PW}, $\{Mo_{72}V_{30}\}$, and $\{Mo_{72}Fe_{30}\}$ were synthesized and purified according to previous literature.[36-39] D. I. water were obtained from Milli-Q water purification system. Infrared spectra (IR) were recorded as KBr pellets on a Nicolet 510 FT-IR. For TEM measurements, the bright-field images of were recorded on a digital CCD camera in JEOL-1230 microscope with an accelerating voltage of 120 keV. A commercial Brookhaven Instrument LLS spectrometer equipped with a solid-state laser operating at 637 nm was used for measurement of DLS.

The preparation of POM-P4VP complex

The P4VP stock solution was prepared by dissolving P4VP in ethanol to a concentration of 2 mg/mL. For the POM solution, the quantity of POM used in the preparation of the aqueous solution was calculated according to molar ratio of POM ({SW}, 1.4~2.0 mg; {PW}, 1.4~2.0 mg; $\{Mo_{72}V_{30}\}$, 1.6~2.0 mg; $\{Mo_{72}Fe_{30}\}$, 1.6~2.0 mg; {Keg}, 0.4~2.0 mg) to P4VP. 1 mL of the P4VP stock solution was drop-wisely added to 10 mL aqueous solutions of certain POM sample while the POM solution was kept vigorously stirring. The obtained solution was kept stirring for another 1 h and the solution was left open to air for overnight.

SAXS experiments

The complex solution was concentrated to *ca.* 1 mL using Macrosep Advance Centrifugal Device (10 K MWCO). The SAXS experiments of these concentrated solution were performed in capillary at 12-ID-B

and C beamline at the Advanced Photon Source of the Argonne National Laboratory. The sample to detector distance was about 2 m. A Pilatus detector (Dectris Ltd.) was used to acquire images with typical exposure times in the range of 0.1 s.

Conclusions

Nanoscale POM clusters strongly associate and stabilize with P4VP polymers in aqueous solutions and form core-shell structures. The core of P4VP interacted with hydroxyl/water sites on POM surface *via* hydrogen bonding, which driving the formation of core-shell NPs. The size of the core-shell was defined by the electrostatic repulsion among POMs in the shell structures. The particle size was tunable upon the introduction of extra salts because of its screening effect to the repulsive interactions. Our POM/polymer complexation protocol provided a convenient way to prepare POM-based quasi-homogeneous catalysts and bio-compatible materials. The test of catalytic efficiency and recyclability of these complex structures is currently undergoing in our lab.

Conflicts of interest

There are no conflicts of interest to declare

Acknowledgements

P. Y. is grateful to the support of the Program for Guangdong Introducing Innovative and Entrepreneurial Teams (No.2016ZT06C322), the Thousand Talents Plan for Young Professionals from Chinese Government, and the startup support from South China University of Technology. T. Liu acknowledges support from the NSF (CHE1607138) and the University of Akron.Use of the Center for Nanoscale Materials and the synchrotron-based SAXS study in 12-ID-C of the Advanced Photon Source, both are U.S. Department of Energy (DOE) Office of Science User Facility operated for the DOE Office of Science by Argonne National Laboratory under Contract No. DE-AC02-06CH11357. This material is based upon work supported by Laboratory Directed Research and Development (LDRD) funding from Argonne National Laboratory, provided by the Director, Office of Science, of the U.S. Department of Energy under Contract No. DE-AC02-06CH11357.

Notes and references

1. S. A. Jenekhe, *Science*, 1998, **279**, 1903-1907.
2. N. Fujita, T. Yamashita, M. Asai and S. Shinkai, *Angew. Chem., Int. Ed. Engl.*, 2005, **44**, 1257-1261.
3. Z. C. Sun, F. Bai, H. M. Wu, S. K. Schmitt, D. M. Boye and H. Y. Fan, *J. Am. Chem. Soc.*, 2009, **131**, 13594-+.
4. S. Sanwaria, A. Horechyy, D. Wolf, C.-Y. Chu, H.-L. Chen, P. Formanek, M. Stamm, R. Srivastava and B. Nandan, *Angew. Chem. Int. Ed.*, 2014, **53**, 9090-9093.
5. Y. Zhao, K. Thorkelsson, A. J. Mastroianni, T. Schilling, J. M. Luther, B. J. Rancatore, K. Matsunaga, H. Jinnai, Y. Wu, D. Poulsen, J. M. Frechet, A. P. Alivisatos and T. Xu, *Nat. Mater.*, 2009, **8**, 979-985.
6. X. Pang, Y. He, J. Jung and Z. Lin, *Science*, 2016, **353**, 1268-1272.
7. R. M. Crooks, M. Zhao, L. Sun, V. Chechik and L. K. Yeung, *Acc. Chem. Res.*, 2001, **34**, 181-190.
8. P. Maury, M. Escalante, D. N. Reinhoudt and J. Huskens, *Adv. Mater.*, 2005, **17**, 2718-2723.
9. M. Zhang, M. Drechsler and A. H. E. Müller, *Chem. Mater.*, 2004, **16**, 537-543.
10. A. C. Balazs, T. Emrick and T. P. Russell, *Science*, 2006, **314**, 1107-1110.
11. M. E. Mackay, A. Tuteja, P. M. Duxbury, C. J. Hawker, B. Van Horn, Z. Guan, G. Chen and R. S. Krishnan, *Science*, 2006, **311**, 1740-1743.
12. J. A. Balmer, O. O. Mykhaylyk, S. P. Armes, J. P. A. Fairclough, A. J. Ryan, J. Gummel, M. W. Murray, K. A. Murray and N. S. J. Williams, *J. Am. Chem. Soc.*, 2011, **133**, 826-837.
13. F. Caruso, *Adv. Mater.*, 2001, **13**, 11-22.
14. D. Sunday, J. Ilavsky and D. L. Green, *Macromolecules*, 2012, **45**, 4007-4011.
15. T. Tozawa, J. T. A. Jones, S. I. Swamy, S. Jiang, D. J. Adams, S. Shakespeare, R. Clowes, D. Bradshaw, T. Hasell, S. Y. Chong, C. Tang, S. Thompson, J. Parker, A. Trewin, J. Bacsa, A. M. Z. Slawin, A. Steiner and A. I. Cooper, *Nat. Mater.*, 2009, **8**, 973.
16. S. Bhattacharya and S. K. Samanta, *Chem. Rev.*, 2016, **116**, 11967-12028.
17. J. B. Carroll, B. L. Frankamp and V. M. Rotello, *Chem. Commun.*, 2002, 1892-1893.
18. T. Li, B. Ye, Z. W. Niu, P. Thompson, S. Seifert, B. Lee and Q. Wang, *Chem. Mater.*, 2009, **21**, 1046-1050.
19. A. D. Celiz, T.-C. Lee and O. A. Scherman, *Adv. Mater.*, 2009, **21**, 3937-3940.
20. C. Wang, H. Wu, Z. Chen, M. T. McDowell, Y. Cui and Z. Bao, *Nat. Chem.*, 2013, **5**, 1042.
21. J. Kao and T. Xu, *J. Am. Chem. Soc.*, 2015, **137**, 6356-6365.
22. M. Kopp, S. Kollenda and M. Epple, *Acc. Chem. Res.*, 2017, **50**, 1383-1390.
23. M.-C. Daniel and D. Astruc, *Chem. Rev.*, 2004, **104**, 293-346.
24. L. Cronin and A. Müller, *Chem. Soc. Rev.*, 2012, **41**, 7333-7334.
25. A. Müller and P. Gouzerh, *Chem. Soc. Rev.*, 2012, **41**, 7431-7463.
26. P. Yin, D. Li and T. Liu, *Chem. Soc. Rev.*, 2012, **41**, 7368-7383.
27. P. Yin, A. Bayaguud, P. Cheng, F. Haso, L. Hu, J. Wang, D. Vezenov, R. E. Winans, J. Hao, T. Li, Y. Wei and T. Liu, *Chem. Eur. J.*, 2014, **20**, 9589-9595.
28. B. Li, W. Li, H. Li and L. Wu, *Acc. Chem. Res.*, 2017, **50**, 1391-1399.
29. B. Weifeng, U. Sayaka and M. Noritaka, *Angew. Chem. Int. Ed.*, 2009, **48**, 8281-8284.
30. Q. Zhang, Y. Liao and W. Bu, *Langmuir*, 2013, **29**, 10630-10634.
31. S.-S. Wang and G.-Y. Yang, *Chem. Rev.*, 2015, **115**, 4893-4962.
32. J. M. Clemente-Juan, E. Coronado and A. Gaita-Arino, *Chem. Soc. Rev.*, 2012, **41**, 7464-7478.
33. Y.-F. Song and R. Tsunashima, *Chem. Soc. Rev.*, 2012, **41**, 7384-7402.
34. H. Lv, Y. V. Geletii, C. Zhao, J. W. Vickers, G. Zhu, Z. Luo, J. Song, T. Lian, D. G. Musaev and C. L. Hill, *Chem. Soc. Rev.*, 2012, **41**, 7572-7589.
35. J. T. Rhule, C. L. Hill, D. A. Judd and R. F. Schinazi, *Chem. Rev.*, 1998, **98**, 327-358.
36. Z.-M. Zhang, S. Yao, Y.-G. Li, X.-B. Han, Z.-M. Su, Z.-S. Wang and E.-B. Wang, *Chem. Eur. J.*, 2012, **18**, 9184-9188.
37. M. H. Alizadeh, S. P. Harmalker, Y. Jeannin, J. Martin-Frere and M. T. Pope, *J. Am. Chem. Soc.*, 1985, **107**, 2662-2669.
38. B. Botar, P. Kogerler and C. L. Hill, *Chem. Commun.*, 2005, 3138-3140.
39. A. Müller, E. Krickemeyer, S. K. Das, P. Kögerler, S. Sarkar, H. Bögge, M. Schmidtmann and S. Sarkar, *Angew. Chem. Int. Ed.*, 2000, **39**, 1612-1614.
40. M. Pope, *Heteropoly and Isopoly Oxometalates*, Springer-Verlag Berlin Heidelberg, Berlin, 1983.
41. T. Li, A. J. Senesi and B. Lee, *Chem. Rev.*, 2016, **116**, 11128-11180.
42. T. Li, B. Ye, Z. Niu, P. Thompson, S. Seifert, B. Lee and Q. Wang, *Chem. Mater.*, 2009, **21**, 1046-1050.
43. A. Müller, E. Krickemeyer, H. Bögge, M. Schmidtmann and F. Peters, *Angew. Chem. Int. Ed.*, 1998, **37**, 3359-3363.
44. N. Suthiwangcharoen, T. Li, L. Wu, H. B. Reno, P. Thompson and Q. Wang, *Biomacromolecules*, 2014, **15**, 948-956.
45. T. Li, L. Wu, N. Suthiwangcharoen, M. A. Bruckman, D. Cash, J. S. Hudson, S. Ghoshroy and Q. Wang, *Chem. Commun.*, 2009, 2869-2871.
46. T. Li, Z. Niu, T. Emrick, T. P. Russell and Q. Wang, *Small*, 2008, **4**, 1624-1629.
47. J. Ruokolainen, J. Tanner, O. Ikkala, G. ten Brinke and E. L. Thomas, *Macromolecules*, 1998, **31**, 3532-3536.
48. H. Etxeberria, R. Fernandez, I. Zalakain, I. Mondragon, A. Eceiza and G. Kortaberria, *J. Colloid Interface Sci.*, 2014, **416**, 25-29.
49. A. Sidorenko, I. Tokarev, S. Minko and M. Stamm, *J. Am. Chem. Soc.*, 2003, **125**, 12211-12216.
50. S. Liu and T. Xu, *Macromolecules*, 2016, **49**, 6075-6083.
51. Y. Wang and I. A. Weinstock, *Chem. Soc. Rev.*, 2012, **41**, 7479-7496.

Journal Name

ARTICLE